NUMERICAL STUDY OF STATISTICAL BEHAVIORS OF GALACTIC COSMIC RAYS INVADING THE HELIOSPHERE*

Kotaro Yoshida[a], Shuichi Matsukiyo[b,c], Haruichi Washimi[c]
Tohru Hada[b,c]

[a]Interdisciplinary Graduate School of Engineering Sciences, Kyushu University
Kasuga, 816-8580, Japan
[b]Faculty of Engineering Sciences, Kyushu University, Kasuga, 816-8580, Japan
[c]International Center for Space Weather Science and Education, Kyushu University, Motooka, Nishi-Ku, Fukuoka, 819-0395, Japan

Received 15 April 2022, accepted 16 May 2022,
published online 9 September 2022

The statistics of galactic cosmic rays (GCRs) invading the heliosphere are investigated using numerical simulations. First, a time stationary global heliosphere is reproduced using an MHD simulation. Then, motions of a large number of GCR protons with initial Lorentz factor 10 (~ 10 GeV) and 1000 (~ 1 TeV), distributed in the interstellar space around the heliosphere, are numerically solved. We map the positional distribution of the GCRs arriving at 50 AU from the Sun. Our results show that the arrival position of GCRs depends on their energies. We discuss the statistical behavior of the arriving GCRs at each energy.

DOI:10.5506/APhysPolBSupp.15.3-A20

1. Introduction

Galactic cosmic rays (GCRs) observed on the ground or near the Earth provide us with information to understand the global heliospheric structures. It is well known that the GCRs spectrum below several ten GeV is strongly modified by the solar activities. Voyager 1 directly observed the significant change of the spectral intensity between the inside and outside of the heliosphere [1]. Also, well known is the directional anisotropy of TeV CRs arriving at the Earth. The observed anisotropy (relative intensity) is known to be 10^{-4} to 10^{-3} (*e.g.* [2–4]).

We have presented the trajectory analysis of GCR protons invading the heliosphere using an MHD simulation and a test particle simulation [5]. We showed that the GCR trajectories are characterized by the relative scale

* Presented at the 28th Cracow Epiphany Conference on *Recent Advances in Astroparticle Physics*, Cracow, Poland, 10–14 January, 2022.

between the GCR gyroradii and heliospheric structures. In this paper, we focus on the statistical behavior of the GCRs arriving deep inside the heliosphere to investigate the effect of heliospheric boundary structures on GCR statistics in the level of particle trajectories. After briefly presenting simulation settings and statistical analysis method, we show our analysis results and discuss a statistical tendency of the GCRs with initial Lorentz factor 10 ($\sim$ 10 GeV) and 1000 ($\sim$ 1 TeV).

2. Model

2.1. Simulation settings

The MHD simulation assumes the steady solar wind, whose magnetic moment has north polarity (solar magnetic field in the northern hemisphere is directed outward from the Sun) with the zero tilt angle. The basic algorithm is described in [6]. Simulation parameters are as follows. The solar wind velocity, density, magnetic field strength, and temperature at 1 AU are set to be 400 km/s, 5.0/cc, 50 μG, and 10^5 K, respectively. These quantities are all assumed to be constant in time, and they are simply extrapolated to the inner boundary of the simulation at 50 AU from the Sun. For the outer boundary at 900 AU, the corresponding parameters of the stationary interstellar plasma are 23 km/s, 0.1/cc, 6,300 K, and 3 μG, respectively. Using the above parameters, the simulation is performed until a steady-state heliosphere is reproduced. The details of the simulation results are described in Fig. 1 of [5].

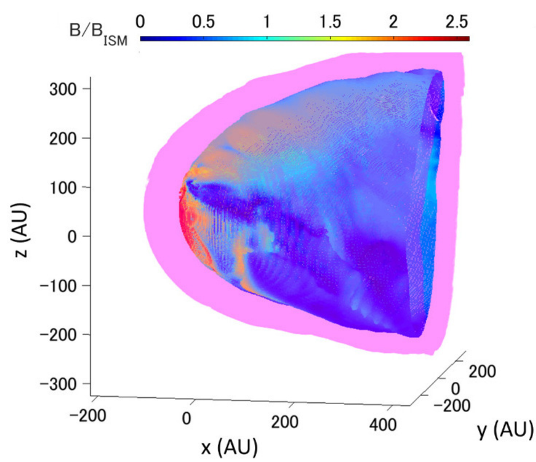

Fig. 1. (Color online) Initial positions of the GCRs with initial Lorentz factor $\gamma = 1000$ (magenta surface). The rainbow-colored surface denotes an iso-temperature surface of $T = 57{,}500$ K, which is defined as the heliopause. The rainbow color of the heliopause denotes magnetic field strength normalized to $B_{\rm ISM} = 3$ μG in the interstellar space.

Using the data obtained from the MHD simulation, we perform a test particle simulation to compute the GCR trajectories. Test particles (GCR protons) are initially distributed on a surface outside the heliopause, which is away from the heliopause by a distance of the typical GCR gyroradius (indicated by the magenta surface in Fig. 1). The number of GCRs is 3×10^6. The heliopause is defined as the iso-temperature surface of 57,500 K. In Fig. 1, the color of the heliopause denotes magnetic field strength normalized to $B_{\mathrm{ISM}} = 3\ \mu$G. The initial velocity distribution function of the GCRs is given by a mono-energetic shell distribution. We performed two runs with different GCRs Lorentz factors, $\gamma = 10$ (~ 10 GeV) and $\gamma = 1000$ (~ 1 TeV). In the following, we analyze the statistics of the GCRs that reached the inner boundary.

2.2. Statistical analysis method

In our simulation, GCRs are uniformly distributed on the initial surface (Fig. 1), and also distributed uniformly on the shell distribution in the velocity space. Figure 2 (a) shows the latitude–longitude distribution of the initial GCRs shown in Fig. 1. Horizontal and vertical axes are the longitude ϕ and the latitude θ, respectively. The longitude ϕ is defined so that $90^\circ \leq \phi \leq 270^\circ$ ($0^\circ \leq \phi < 90^\circ$, $270^\circ < \phi < 360^\circ$) corresponds to the nose (tail) region of the heliosphere. The latitude θ is defined so that $\theta > 0$ (< 0) corresponds to the northern (southern) hemisphere. As shown in Fig. 2 (a), there is an eminent anisotropy in the initial directional distribution. This initial anisotropy should be compensated when we discuss GCR statistics. Thus, we need to apply a weighting function to all the GCR so that the initial distribution becomes uniform. Figure 2 (b) is the initial directional distribution after applying the weighting function. GCR statistics at the end of the simulation were evaluated using the same weighting function. Note that there is a region in the tail where no initial GCRs are present.

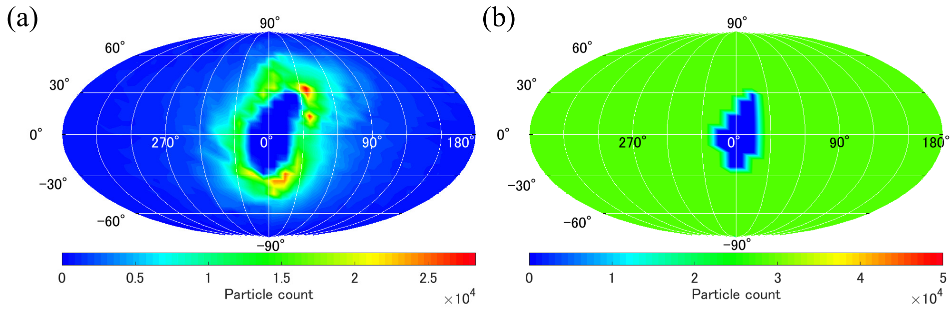

Fig. 2. Latitude–longitude distribution of the initial GCRs (a) before and (b) after applying weighting function. The region $90^\circ \leq \phi \leq 270^\circ$ ($0^\circ \leq \phi < 90^\circ$, $270^\circ < \phi < 360^\circ$) corresponds to the nose (tail) region of the heliopshere.

3. Simulation results

3.1. $\gamma = 10$ ($\sim$ 10 GeV)

Figure 3 (a) shows the distribution of the arrival position on the inner boundary (the same format as Fig. 2). It is clear that many GCRs reached the mid-high latitudes, $-90° \leq \phi \leq -45°$ or $45° \leq \phi \leq 90°$. Figure 3 (b) shows the sample trajectories of GCRs that arrived in the northern hemisphere projected onto the meridional plane at $y = 0$ AU. The (background) gray scale denotes the magnetic field strength. Two types of propagation patterns are confirmed. The first type is the GCRs coming from the high latitudes. Spiral magnetic fields emanate from the Sun and eventually trail the tailward. The center of the spiral fields is a current vortex. The GCRs following the spiral magnetic field are finally captured by the current vortex and reach the inner boundary near the pole. The second type of GCRs comes from the equatorial current sheet. When the GCRs propagating around the current sheet approach the inner boundary, they drift poleward along the termination shock. There are two drift patterns, due to the shock drift and the drift combined with Fermi-like acceleration, as discussed in [5].

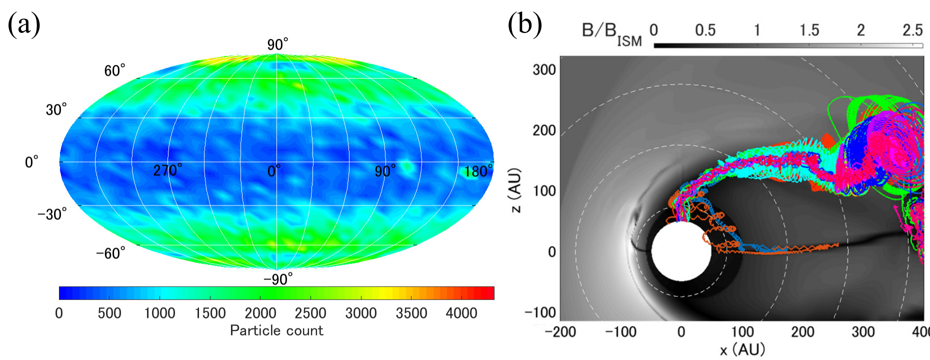

Fig. 3. Simulation results for $\gamma = 10$ ($\sim$ 10 GeV). (a) The distribution of the arrival position on the inner boundary, (b) the sample trajectories of GCRs which arrived in the northern hemisphere projected onto the meridional plane at $y = 0$ AU.

3.2. $\gamma = 1000$ ($\sim$ 1 TeV)

Figure 4 (a) shows the simulation results for $\gamma = 1000$, given in the same format as Fig. 3 (a). There is a clear concentration of GCRs in the tail region, suggesting that many GCRs come from the tail part of the heliosphere. Moreover, there is a tendency that more GCRs reach the low-mid latitudes, $-60° < \theta < 60°$. Figure 4 (b) shows sample trajectories of GCRs that arrived at the region (the same format as Fig. 3 (b)). These GCRs are roughly confined in the tail region where the magnetic field is relatively weak. Figures 4 (c) and (d) show one of the trajectories projected onto the meridional plane at $y = 0$ AU and the plane at $x = 200$ AU. The local spiral magnetic field of the solar wind in the plane at $x = 200$ AU is indicated by the white arrows in Fig. 4 (d). The center of the red dotted circle corresponds to the current vortex. The corresponding position in Fig. 4 (c) is also indicated by the red dotted circle. In this projection, the GCR motion is similar to the meandering motion. Due to its large gyroradius, the GCR threads its way along the current vortex. When GCRs finally reach the inner boundary, they are excluded from the polar region.

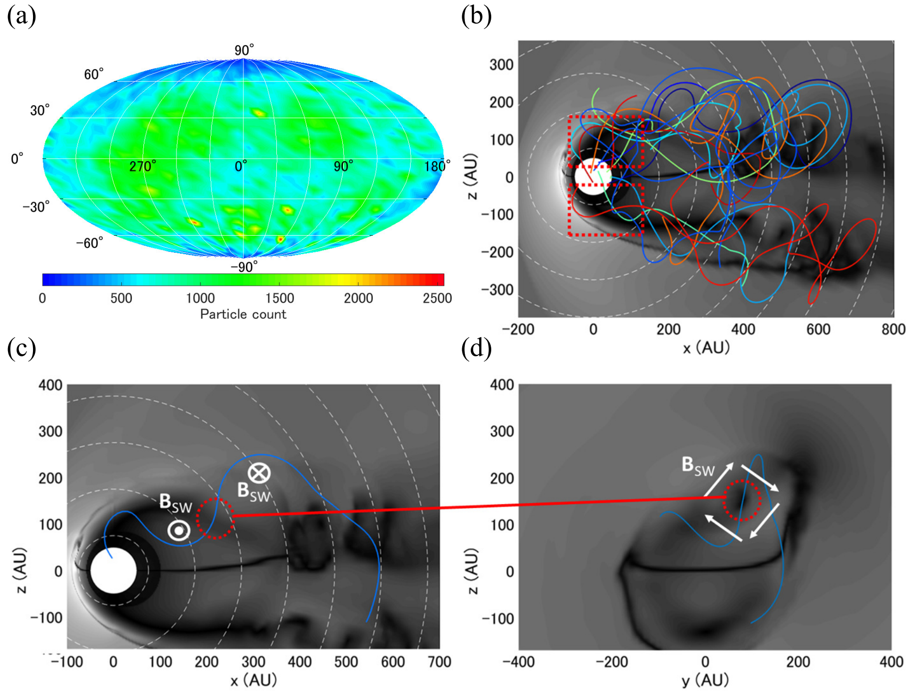

Fig. 4. (Color online) Simulation results of $\gamma = 1000$ (~ 1 TeV). (a) and (b) are given in the same format as Fig. 3 (a) and (b). (c) and (d) show a typical trajectory projected onto the meridional plane at $y = 0$ AU and the plane at $x = 200$ AU. Local spiral magnetic field $\boldsymbol{B}_{\mathrm{SW}}$ of the solar wind in the plane at $x = 200$ AU is indicated by the white arrows in (d). The center of the red dotted circle corresponds to the current vortex.

4. Summary

We have investigated the statistical behavior of the GCR protons with $\gamma = 10$ (~ 10 GeV) and $\gamma = 1000$ (~ 1 TeV) arriving deep inside the virtual heliosphere reproduced by an MHD simulation. A weighting function was introduced to evaluate the anisotropy of arriving position of the GCRs at the inner boundary at 50 AU from the Sun.

The GCRs with $\gamma = 10$ tend to arrive in the mid-high latitude region of the inner boundary. We confirmed that there are two arrival patterns. The first type of the GCRs follows a spiral magnetic field in the tail region to be then captured by the polar current vortex. The second type of the GCRs initially propagates in the equatorial current sheet and then drifts poleward along the termination shock. During the poleward drift, the GCRs are accelerated through the shock drift mechanism.

The GCRs with $\gamma = 1000$ tend to arrive at the mid-low latitude of the tail region. As in the case of $\gamma = 10$, we found that many GCRs come from high latitudes while moving around the current vortex. GCRs with large gyroradius precipitate along the polar current vortex. The projection of their motion in the meridional plane ($y = 0$ AU) shows the feature similar to the meandering motion. They finally reach the mid-low latitude of the inner boundary.

To make a more reliable comparison with observations, we need to increase the number of GCRs and obtain higher statistics. For the MHD simulation, the effect of the finite tilt angle of the Sun's magnetic moment should be incorporated. The polarity of the magnetic moment is fixed in the present study, but it is reversed every 11 years in reality. The solar wind is not time stationary, and moreover, the solar wind is abundant with large amplitude waves and turbulence. This should cause pitch angle scattering of GCRs.

This work was supported by JST SPRING, grant Number JPMJSP2136, and Grant-in-Aid for Scientific Research (C) No. 19K03953 and 22H01287 from JSPS (S.M.).

REFERENCES

[1] Q. Yuan, «Implications on cosmic ray injection and propagation parameters from Voyager/ACE/AMS-02 nucleus data», *Sci. China Phys. Mech.* **62**, 49511 (2019).
[2] R. Abbasi *et al.*, «Observation of Anisotropy in the Galactic Cosmic-Ray Arrival Directions at 400 TeV with IceCube», *Astrophys. J.* **746**, 33 (2012).
[3] Tibet AS Collaboration (M. Amenomori *et al.*), «Northern Sky Galactic Cosmic Ray Anisotropy between 10 and 1000 TeV with the Tibet Air Shower Array», *Astrophys. J.* **836**, 153 (2017).
[4] M. Zhang *et al.*, «The Original Anisotropy of TeV Cosmic Rays in the Local Interstellar Medium», *Astrophys. J.* **889**, 97 (2020).
[5] K. Yoshida *et al.*, «Trajectory Analysis of Galactic Cosmic Rays Invading into the Heliosphere», *Astrophys. J.* **916**, 29 (2021).
[6] H. Washimi *et al.*, «MHD Modeling of the Outer Heliospheric Structures around the Heliopause», *Astrophys. J.* **809**, 16 (2015).